Terahertz surface plasmons in optically pumped graphene structures

2011 J. Phys.: Condens. Matter 23 145302

(http://iopscience.iop.org/0953-8984/23/14/145302)

J. Phys.: Condens. Matter **23** (2011) 145302 (8pp) doi:10.1088/0953-8984/23/14/145302

Terahertz surface plasmons in optically pumped graphene structures

A A Dubinov[1,2], V Ya Aleshkin[2], V Mitin[3], T Otsuji[4,5] and V Ryzhii[1,5]

[1] Computational Nanoelectronics Laboratory, University of Aizu, Aizu-Wakamatsu 965-8580, Japan
[2] Institute for Physics of Microstructures, Russian Academy of Sciences, Nizhny Novgorod 603950, Russia
[3] Department of Electrical Engineering, University at Buffalo, State University of New York, NY 14260, USA
[4] Research Institute for Electrical Communication, Tohoku University, Sendai 980-8577, Japan
[5] Japan Science and Technology Agency, CREST, Tokyo 107-0075, Japan

Received 12 January 2011, in final form 1 March 2011
Published 25 March 2011
Online at stacks.iop.org/JPhysCM/23/145302

Abstract
We analyze the surface plasmons (SPs) propagating along optically pumped single-graphene layer (SGL) and multiple-graphene layer (MGL) structures. It is shown that at sufficiently strong optical pumping when the real part of the dynamic conductivity of SGL and MGL structures becomes negative in the terahertz (THz) range of frequencies due to the interband population inversion, the damping of the THz SPs can give way to their amplification. This effect can be used in graphene-based THz lasers and other devices. Due to the relatively small SP group velocity, the absolute value of their absorption coefficient (SP gain) can be large, substantially exceeding that of optically pumped structures with dielectric waveguides. A comparison of SGL and MGL structures shows that to maximize the SP gain the number of graphene layers should be properly chosen.

(Some figures in this article are in colour only in the electronic version)

1. Introduction

Optical excitation of graphene can result in interband population inversion [1, 2]. At sufficiently strong excitation, the interband emission of photons can prevail over the intraband (Drude) absorption. In this case, the real part of the dynamic conductivity $\mathrm{Re}\,\sigma_\omega$ becomes negative. Due to the gapless energy spectrum of graphene [3], $\mathrm{Re}\,\sigma_\omega$ can be negative at relatively low frequencies ω, for instance, those in the terahertz (THz) range. This effect can be used in graphene-based THz optically pumped lasers with Fabry–Pérot resonators and resonators based on dielectric or slot-line waveguides [4–6]. As was previously pointed out [1] and analyzed [7], apart from the lasing associated with the stimulated generation of electromagnetic modes, the stimulated generation of different plasmons (with their conversion into electromagnetic radiation) can also be of practical interest. The plasma excitations in graphene associated with the electrons and holes in the conduction and valence bands, respectively, were considered, in particular, in [8–14]. In particular, in [13, 14], electromagnetic surface plasmons (SPs) with the electric and magnetic fields located near a graphene layer were studied; in the latter paper, the propagation and damping of SPs in the equilibrium electron–hole system. In this paper, we study the propagation of electromagnetic SPs in graphene structures under nonequilibrium conditions when $\mathrm{Re}\,\sigma_\omega < 0$ due to optical pumping and, as demonstrated, amplification is possible. We consider single-graphene layer (SGL) and multiple-graphene layer (MGL) structures on a substrate. As demonstrated recently (see the review paper [15] and references therein), the MGLs, which constitute stacks of disoriented (non-Bernal stacked) graphene layers (GLs), exhibit similar electron and optical properties to individual GLs, while the electron momentum relaxation time in such MGLs can be extremely long. The latter circumstance implies that the intraband absorption of photons and plasmons can be effectively diminished. This makes the MGLs good prospects for different optoelectronic devices considering that the net dynamic conductivity along GLs increases with

increasing their number in the MGL structure. MGL structures can be particularly effective in lasers in which the THz modes are supported by the external resonator or waveguide [5, 6], THz photodetectors [16–18], and transit-time THz oscillators [19, 20]. However, SGL and MGL structures can play a dual role: the imaginary part of their dynamic conductivity provides the mode localization near the SGL or MGL (i.e., the formation of SPs), while the real part provides absorption or amplification of SPs. Due to this, MGL structures as SP waveguides are not always superior over SGL structures.

Since the thickness, d, of an MGL structure with even relatively large number, K, of GLs is rather small in comparison with the wavelength of SPs under consideration, we shall consider the SGL and MGL structures alike. Real MGL structures usually include a highly conducting bottom GL (at the interface between the substrate and the other GLs) with rather high electron density [15, 21]. Although this bottom GL can be in some way removed, we will take it into account.

It is assumed that the SGL or MGL structure is illuminated from the top by light with the energy of photons $\hbar\Omega$, and SPs propagate along the SGL/MGL plane as shown in figure 1. Under optical excitation, the electron and hole densities exceed substantially their equilibrium values. Due to this, one can consider the electron and hole systems under consideration as characterized by the quasi-Fermi energies $\pm\varepsilon_{\rm F}^{(k)}$, respectively, and the effective temperature T. A distinction in the Fermi energies in GLs with different indices is due to the attenuation of incident optical radiation associated with its absorption in the GLs closer to the top of the structure: $\varepsilon_{\rm F}^{(k)} < \varepsilon_{\rm F}^{(K)} = \varepsilon_{\rm F}^{\rm T}$. The electron–hole system in the bottom GL in MGLs is characterized by the unified Fermi energy $\varepsilon_{\rm F}^{\rm B}$ determined by the doping of this GL. If the characteristic time, τ_0, of the emission of the optical phonon by an electron or a hole is much shorter than the time of pair collisions, the photoexcited electrons and holes emit a cascade of optical phonons and occupy low energy states in the conduction and valence bands, respectively. In this case, the contribution of optical excitation to the heating of the electron–hole system is small, so that the effective temperature T is close to the lattice temperature $T_{\rm l}$ [22]. Moreover, some cooling of the electron–hole system can occur [23]. In the opposite case, the photoexcited electrons and holes are thermalized, and their effective temperature is determined by the pumping photon energy $\hbar\Omega$ and the rate of electron and hole energy relaxation. In such a situation, the effective temperature can be elevated, so that somewhat stronger optical pumping might be needed to fulfil the condition Re $\sigma_\omega < 0$ [23, 24].

2. Dynamic conductivity of SGL and MGL structures

The net dynamic conductivity in the lateral direction of a structure with K GLs at the signal frequency ω can be presented as the sum of the contributions of the individual GLs $\sigma_\omega^{(k)}$ ($k = 1, 2, \ldots, K$) and the bottom GL $\sigma_\omega^{\rm B}$:

$$\sigma_\omega = \sum_{k=1}^{K} \sigma_\omega^{(k)} + \sigma_\omega^{\rm B}. \tag{1}$$

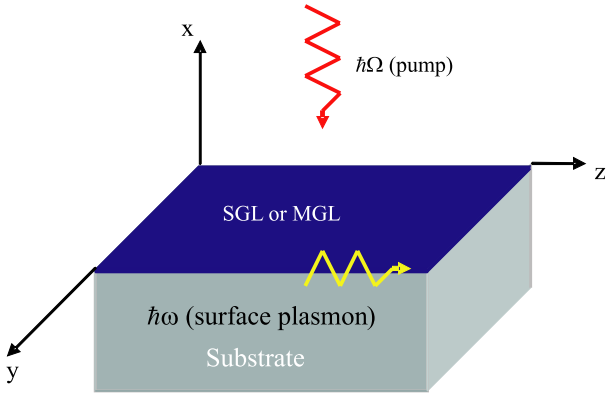

Figure 1. Schematic view of the SGL/MGL structure under consideration. Wavy arrows show the direction of incidence of pumping radiation (perpendicular to the SGL/MGL plane) with photon energy $\hbar\Omega$ and the direction of propagation (along this plane) of SPs with frequency ω.

Considering the expressions for $\sigma_\omega^{(k)}$ and $\sigma_\omega^{\rm B}$ obtained previously (see, for instance, [10, 25], as well as the recent review paper [26]), one can arrive at the following:

$$\sigma_\omega^{(k)} = \left(\frac{e^2}{4\hbar}\right)\left\{\frac{8k_{\rm B}T\tau}{\pi\hbar(1-{\rm i}\omega\tau)}\ln\left[1+\exp\left(\frac{\varepsilon_{\rm F}^{(k)}}{k_{\rm B}T}\right)\right] + \tanh\left(\frac{\hbar\omega-2\varepsilon_{\rm F}^{(k)}}{4k_{\rm B}T}\right) - \frac{4\hbar\omega}{{\rm i}\pi}\int_0^\infty \frac{G(\varepsilon,\varepsilon_{\rm F}^{k}) - G(\hbar\omega/2,\varepsilon_{\rm F}^{k})}{(\hbar\omega)^2-4\varepsilon^2}\,{\rm d}\varepsilon\right\}, \tag{2}$$

$$\sigma_\omega^{\rm B} = \left(\frac{e^2}{4\hbar}\right)\frac{4k_{\rm B}T\tau_{\rm B}}{\pi\hbar(1-{\rm i}\omega\tau_{\rm B})}\ln\left[1+\exp\left(\frac{\varepsilon_{\rm F}^{\rm B}}{k_{\rm B}T}\right)\right] + \left(\frac{e^2}{4\hbar}\right)\left\{1-\left[1+\exp\left(\frac{\hbar\omega/2-\varepsilon_{\rm F}^{\rm B}}{k_{\rm B}T}\right)\right]^{-1} - \left[1+\exp\left(\frac{\hbar\omega/2+\varepsilon_{\rm F}^{\rm B}}{k_{\rm B}T}\right)\right]^{-1} - \frac{4\hbar\omega}{{\rm i}\pi}\int_0^\infty \frac{G(\varepsilon,\varepsilon_{\rm F}^{\rm B}) - G(\hbar\omega/2,\varepsilon_{\rm F}^{\rm B})}{(\hbar\omega)^2-4\varepsilon^2}\,{\rm d}\varepsilon\right\}. \tag{3}$$

Here, e is the electron charge, $\tau_{\rm B}$ and τ are the electron and hole momentum relaxation times in the bottom and other GLs, respectively, $\hbar$ is the reduced Planck constant, $k_{\rm B}$ is the Boltzmann constant, and

$$G(\varepsilon,\varepsilon') = \frac{\sinh(\varepsilon/k_{\rm B}T)}{\cosh(\varepsilon/k_{\rm B}T)+\cosh(\varepsilon'/k_{\rm B}T)}. \tag{4}$$

In the case of an SGL structure, one should put $K = 1$ and $\sigma_\omega^{\rm B} = 0$. For the MGL structures without the bottom GL, one can use equation (3) formally setting $\sigma_\omega^{\rm B} = 0$.

The quasi-Fermi energies in the GLs with $k \geqslant 1$, $\varepsilon_{\rm F}^{(k)}$, are mainly determined by the electron (hole) density in this layer, Σ_k, with $\varepsilon_{\rm F}^{(k)} \propto \sqrt{\Sigma^{(k)}}$ (at sufficiently strong degeneracy of the electron and hole systems), i.e., by the rate of photogeneration $G_\Omega^{(k)}$ by the optical radiation at the kth GL plane. Considering the attenuation of the optical pumping radiation due to its absorption in each GL, one can obtain

that $\varepsilon_{\rm F}^{(k)}$ can be expressed via the quasi-Fermi energy in the topmost GL, $\varepsilon_{\rm F}^{\rm T} = \varepsilon_{\rm F}^{(K)}$, which, in turn, is a function of the intensity of incident pumping radiation I_Ω. Considering the MGL structures, the $\varepsilon_{\rm F}^{(k)}$ versus $\varepsilon_{\rm F}^{\rm T}$ dependence was found as previously [6].

3. Dispersion equation for SPs

We consider SPs propagating along the z-direction in the plane (yz-plane) of an SGL/MGL structure at the interface between a substrate with the refraction index (generally complex) n and the vacuum (see figure 1). The SP electric and magnetic fields, $\mathbf{E} = (E_x, 0, E_z)$ and $\mathbf{H} = (0, H_y, 0)$, are governed by the Maxwell equations, which in the situation under consideration can be presented in the following form:

$$\nabla \times \mathbf{E} = \frac{1}{c}\frac{\partial \mathbf{H}}{\partial t}, \qquad \nabla \times \mathbf{H} = \frac{4\pi}{c}\mathbf{j} - \frac{n^2}{c}\frac{\partial \mathbf{E}}{\partial t}. \tag{5}$$

Here, c is the speed of light and $\mathbf{j}$ is the density of the current (per unit length in the y-direction), which is created by the electrons and holes under the z-component of the SP electric field E_z. The components of $\mathbf{j}$ are given by

$$j_x = 0, \qquad j_y = 0, \qquad j_z = \sigma_\omega E_z\, \delta(x), \tag{6}$$

where $\delta(x)$ is the Dirac delta function. The latter reflects the fact that the thickness, d, of the MGL structure (and, certainly, of the SGL structure) is much smaller than the width of the SP electric and magnetic field localization near the SGL/MGL plane, and, hence, the current can be considered as localized at $x = 0$.

Searching for the components of the electric and magnetic fields in the form of a wave propagating in the z-direction,

$$\mathbf{E} = \overline{\mathbf{E}} \exp\left(\mathrm{i}\frac{\omega}{c}\sqrt{1-\rho^2}x + \mathrm{i}\frac{\omega}{c}\rho z - \mathrm{i}\omega t\right),$$
$$\mathbf{H} = \overline{\mathbf{H}} \exp\left(\mathrm{i}\frac{\omega}{c}\sqrt{1-\rho^2}\,x + \mathrm{i}\frac{\omega}{c}\rho\, z - \mathrm{i}\omega\, t\right),$$

where $\overline{\mathbf{E}}$ and $\overline{\mathbf{H}}$ are the amplitudes of the fields, equations (5) and (6) can be rewritten as

$$\frac{\partial \overline{E}_z}{\partial x} = \mathrm{i}\frac{\omega}{c}(1-\rho^2)\overline{H}_y \qquad (x \geqslant 0),$$
$$\frac{\partial \overline{E}_z}{\partial x} = \mathrm{i}\frac{\omega}{c}\left(1 - \frac{\rho^2}{n^2}\right)\overline{H}_y \qquad (x < 0), \tag{7}$$
$$\overline{H}_y\Big|_{x=0+} - \overline{H}_y\Big|_{x=0-} = \frac{4\pi}{c}\sigma_\omega \overline{E}_z.$$

Here, ω is the SP frequency and ρ is the complex propagation index (which relates to the wavenumber $q_z = \rho\omega/c$). Solving equations (7), we obtain the following dependences of the amplitudes $\overline{E}_z$ and $\overline{H}_y$ on the coordinate x:

$$\overline{E}_z = A\mathrm{e}^{(\mathrm{i}\frac{\omega}{c}\sqrt{1-\rho^3}x)} \qquad (x \geqslant 0),$$
$$\overline{E}_z = A\mathrm{e}^{(\mathrm{i}\frac{\omega}{c}\sqrt{n^2-\rho^3}x)} \qquad (x < 0),$$
$$\overline{H}_y = B\mathrm{e}^{(\mathrm{i}\frac{\omega}{c}\sqrt{1-\rho^3}x)} \qquad (x \geqslant 0), \tag{8}$$
$$\overline{H}_y = C\mathrm{e}^{(\mathrm{i}\frac{\omega}{c}\sqrt{n^2-\rho^3}x)} \qquad (x < 0),$$

where A, B, and C are constants. As usual, invoking the condition of the existence of a nontrivial solution of the above equations, we arrive at the following dispersion equation for SPs:

$$\sqrt{n^2-\rho^2} + n^2\sqrt{1-\rho^2} + \frac{4\pi}{c}\sigma_\omega\sqrt{1-\rho^2}\sqrt{n^2-\rho^2} = 0. \tag{9}$$

Equation (9) can also be derived using a different approach [13, 14]. It is important for the present consideration that σ_ω is determined by both nonequilibrium electron and hole components with, in particular, $\mathrm{Re}(\sigma_\omega) < 0$. This is in contrast to the studies of SPs in the cases when the electron–hole system is in equilibrium. Solving equation (9) with respect to ρ, one can find the propagation index $\mathrm{Re}(\rho)$ and the SP absorption (amplification) coefficient $2\,\mathrm{Im}(q) = 2\,\mathrm{Im}(\rho\omega/c)$ or the SP gain $-2\,\mathrm{Im}(q)$ as a function of the frequency ω. In the cases when $n = 1$ (SGL or MGL structure levitating in free space), equation (9) obviously yields

$$\rho = \sqrt{1 - \frac{c^2}{4\pi^2\sigma_\omega^2}}. \tag{10}$$

4. Results of calculations

4.1. SP spectra and SP damping/amplification

Figure 2 presents the frequency dependences of the real part of the propagation index $\mathrm{Re}(\rho) \propto \mathrm{Re}(q)$ shown by solid lines, calculated for SGL structures with different substrate refraction indices n at different temperatures T and different values of the quasi-Fermi energies $\varepsilon_{\rm F}^{\rm T}$ (i.e., for different pumping intensities). The electron and hole momentum relaxation time τ was set to be rather long: $\tau = 10$ ps. Such values can be realized in sufficiently perfect MGL structures (see [27], as well as the review paper [15], in which the experimentally obtained value $\tau \simeq 20$ ps at temperatures up to 55 K was reported). Much smaller values of τ ($\tau = 1$, 0.54, and 0.1 ps) were also used in our calculations (see below). The dotted lines in figure 2 correspond to the frequency dependences of the group velocity of SPs normalized by the speed of light in a vacuum, c. In our model we disregarded the effect of spatial dispersion on the dynamic conductivity of SGL and MGL structures, i.e., the dependence of σ_ω on the SP wavenumber q_z in equations (1)–(4). This is valid if $\rho < c/v_{\rm W}$ or $\omega < \mathrm{Re}(q_z)v_{\rm W}$ [10], where $v_{\rm W} = 10^8$ cm s^{-1} is the characteristic velocity of electrons and holes in graphene. In the case of SGL structures with $n = 1$, these inequalities are satisfied in the frequency range under consideration (see figures 2 and 3). However, as follows from figure 2 at larger n, the validity of the dependences obtained is limited by relatively low frequencies ($\omega/2\pi \leqslant$ 5–8 THz for $n = 3.4$ at $T = 300$ K). One can see from figure 2 that the SP group velocity can be negative (at $T = 77$ K) at elevated frequencies. This corresponds to backward waves [28, 29] and occurs at the frequencies at which the imaginary part of the dynamic conductivity is determined primarily by the interband transitions. For convenience, figure 3 shows the spectra of SPs, i.e., ω versus Re (q_z) dependences in the

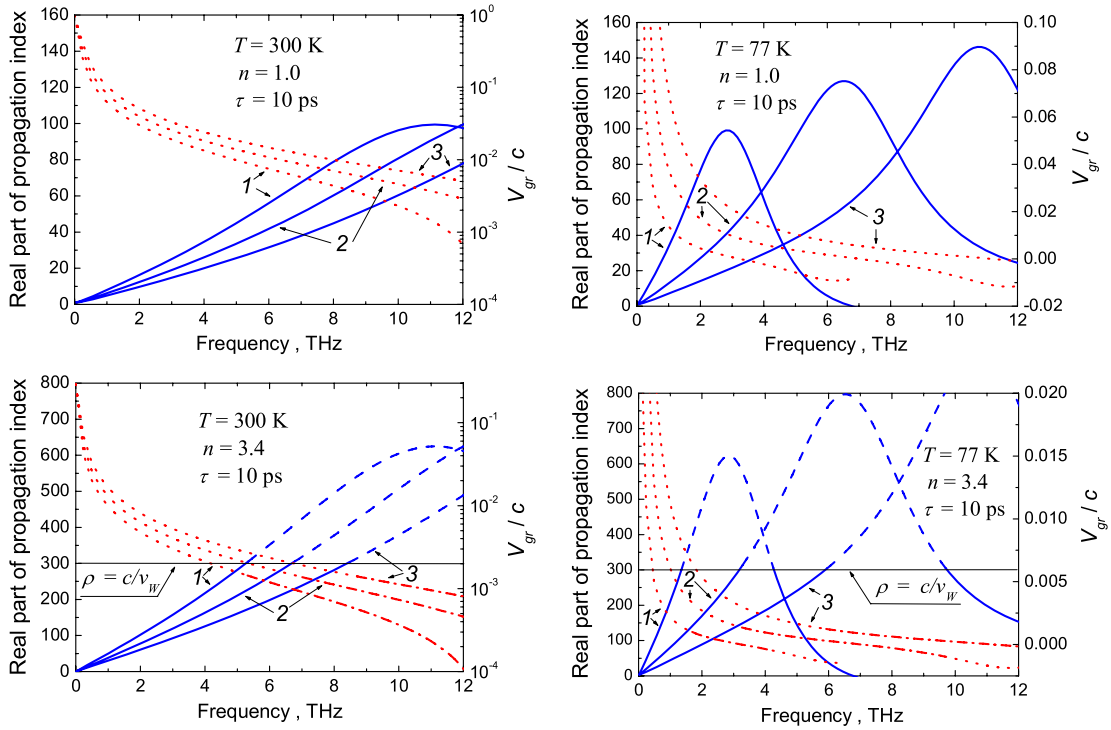

Figure 2. Frequency dependence of the real part of the propagation index Re(ρ) (solid lines) and the SP group velocity normalized by the speed of light (dotted lines) in SGL structures at different temperatures ($T = 300$ and 77 K) and different quasi-Fermi energies (1—$\varepsilon_F^T = 0$ meV, 2—$\varepsilon_F^T = 10$ meV, and 3—$\varepsilon_F^T = 20$ meV) for SGL structures with different substrate refraction indices ($n = 1.0$ and 3.4). The dashed and dashed–dotted lines in the figures for $n = 3.4$ correspond to the ranges where the effects of spatial dispersion might be essential.

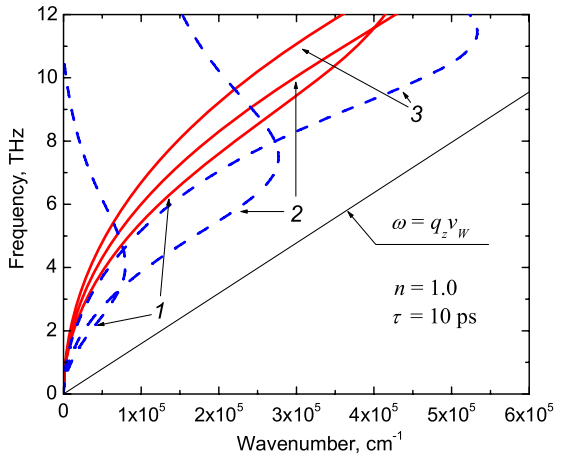

Figure 3. Dispersion of SPs in an SGL structure at $T = 300$ K (solid lines) and $T = 77$ K (dashed lines) with the same values of the quasi-Fermi energy as in figure 2.

SGL structures at different temperatures at the same pumping conditions as in figure 2. As follows from figure 3, SPs with large wavenumbers $q_z \sim 10^5$ cm^{-1} and, hence, with rather short wavelengths $\lambda \sim 1$ μm and less are in the THz range.

Figure 4 shows the SP absorption coefficient 2Im (q_z) as a function of frequency, calculated for different temperatures T and different values of the quasi-Fermi energies ε_F^T. One can see that an increase in ε_F^T leads to widening of the frequency range where Im(q_z) < 0 and a marked increase in the absolute value of the absorption coefficient in this range. The dependences indicated by markers were calculated for equilibrium SGLs using the above formulas, which in the absence of optical pumping at $n = 1$ coincide with those obtained previously [13]. The markers correspond to intrinsic (with the Fermi energy $\varepsilon_F = 0$) and doped SGL structures. The dependences for doped GL structures at equilibrium correspond to the Fermi energies ε_F in doped SGLs at equilibrium equal to the quasi-Fermi energies ε_F^T in the optically pumped SGLs. Clear distinctions in these dependences in the equilibrium and pumped GLs are associated with the contributions of both electrons and holes to the negative dynamic conductivity due to the interband transitions (in the latter).

Figure 5 shows the spatial distributions (in the direction perpendicular to the SGL plane) of the SP electric and magnetic fields in SGL structures with different substrate refraction indices. The obtained spatial distributions demonstrate pronounced localization of the SP electric and magnetic fields near the SGL plane. One can see that an increase in the SP frequency and the substrate refraction index leads to a stronger localization.

4.2. The role of substrate and intraband absorption

Figure 6 shows the frequency dependences of the SP absorption coefficient calculated for SGLs with substrates

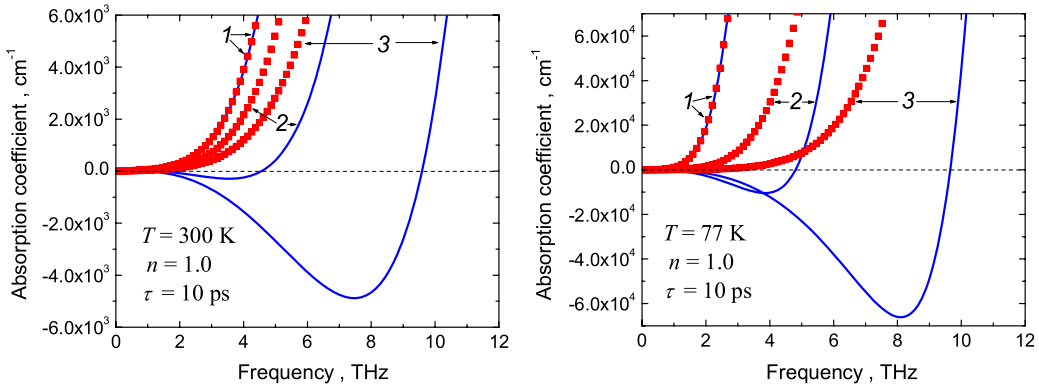

Figure 4. Frequency dependences of the SP absorption coefficient $2\,\mathrm{Im}(q)$ in an SGL structure at $T = 300$ K (left panel) and $T = 77$ K (right panel) and for different quasi-Fermi energies (1—$\varepsilon_F^T = 0$ meV, 2—$\varepsilon_F^T = 10$ meV, and 3—$\varepsilon_F^T = 20$ meV). The markers show the dependences for equilibrium electron–hole systems calculated using the derived formulas as well as using [13] for intrinsic and doped SGL structures.

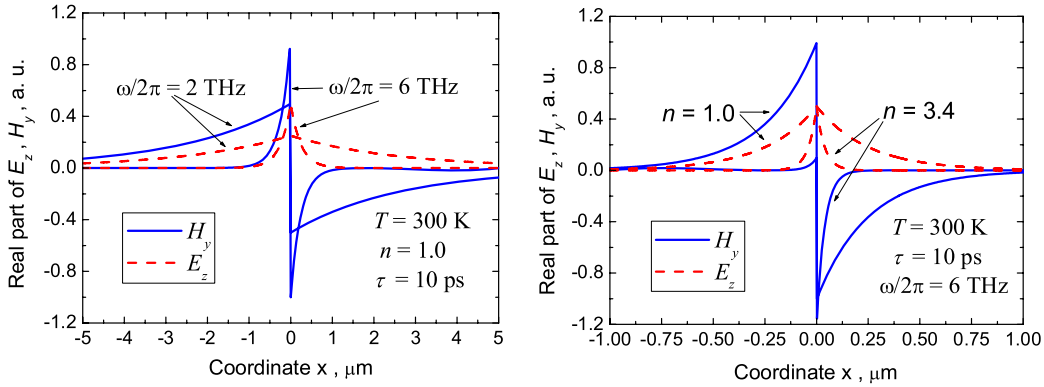

Figure 5. Spatial distributions of the real parts of the electric and magnetic fields in SGL structures at different frequencies (left panel) and different substrate refraction indices (right panel): $T = 300$ K, $\varepsilon_F^T = 20$ meV, and $\tau = 10$ ps.

with different real and imaginary parts of the refraction index (different absorption in the substrate). An increase in the substrate refraction index and, consequently, stronger localization of the SP electric and magnetic fields, as demonstrated in figure 5, results in markedly larger absolute values of the absorption coefficient in the frequency range where it is negative (compare curves 1 and 2 in figure 6). However, as follows from the comparison of curves 2 and 3 in figure 6, the contribution of the substrate to the SP absorption can be relatively weak at realistic values of the imaginary part of the substrate refraction index. In particular, in the case of the substrate made of undoped Si (Im $(n) \simeq 3 \times 10^{-4}$ [30]), the imaginary part of the refraction index can be smaller than those used in the calculations of curves 3–5 in figure 6. Naturally, at large values of the imaginary part of the substrate refraction index corresponding to curves 4 and 5, the effect of the substrate on the SP absorption can be pronounced and lead to a positive net absorption coefficient, i.e., to SP damping.

Figure 7 shows the frequency dependences of the real part of the propagation index and the SP absorption coefficient. These dependences were calculated for SGL structures with different electron and hole momentum relaxation times ($\tau =$ 10 and 0.1 ps) for different ε_F^T, i.e., for different pumping intensities, assuming that $T = 300$ K. As seen from figure 7, in the SGL structure with a relatively long momentum relaxation

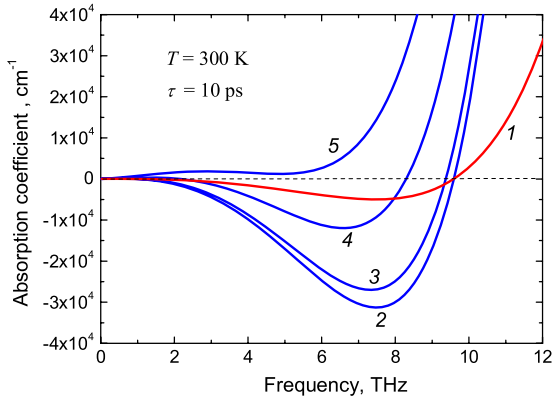

Figure 6. Frequency dependences of SP absorption for SGL structures with different substrate refraction indices n: 1—$n = 1.0$, 2—$n = 3.4$, 3—$n = 3.4 + \mathrm{i}0.01$, 4—$n = 3.4 + \mathrm{i}0.05$, and 5—$n = 3.4 + \mathrm{i}0.1$ ($T = 300$ K, $\varepsilon_F^T = 20$ meV).

time ($\tau = 10$ ps), the SP absorption coefficient changes its sign at moderate values of ε_F^T ($\varepsilon_F^T \leqslant 20$ meV). However when $\tau = 0.1$ ps, the SP absorption coefficient does not change its sign at least at $\varepsilon_F^T \sim 20$ meV (see below), although it is markedly smaller than in the equilibrium conditions (without pumping). However, at elevated pumping intensities (elevated

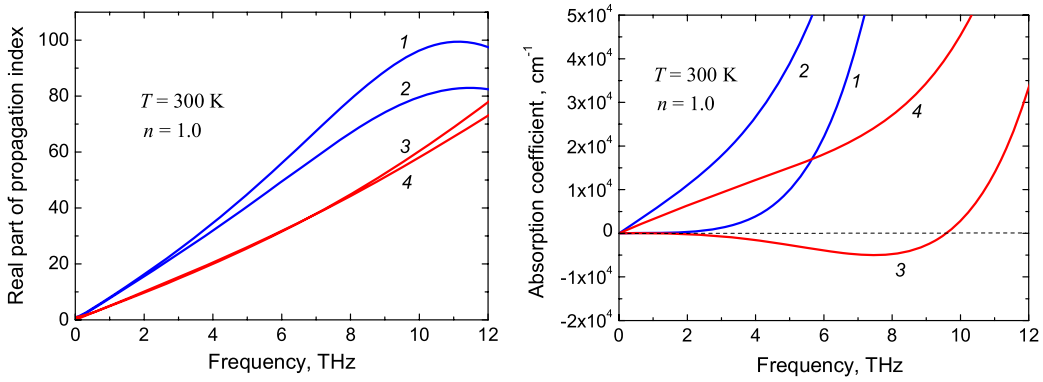

Figure 7. Real part of the SP propagation index (left panel) and absorption coefficient (right panel) in SGL structures as functions of frequency: 1—$\varepsilon_F^T = 0$ meV, $\tau = 10$ ps, 2—$\varepsilon_F^T = 0$ meV, $\tau = 0.1$ ps, 3—$\varepsilon_F^T = 20$ meV, $\tau = 10$ ps, and 4—$\varepsilon_F^T = 20$ meV, $\tau = 0.1$ ps.

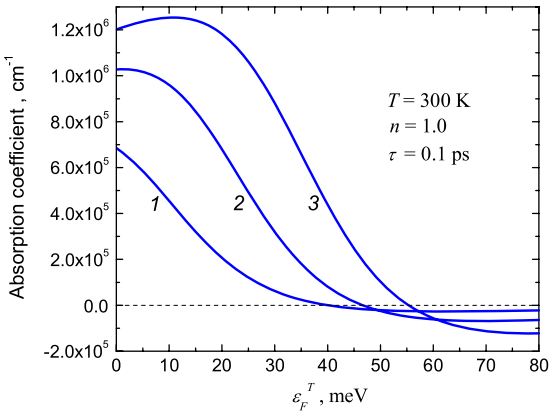

Figure 8. SP absorption coefficient as a function of the quasi-Fermi energy in SGL structures with short momentum relaxation time ($\tau = 0.1$ ps) at 1—$\omega/2\pi = 15$ THz, 2—$\omega/2\pi = 20$ THz, 3—$\omega/2\pi = 25$ THz.

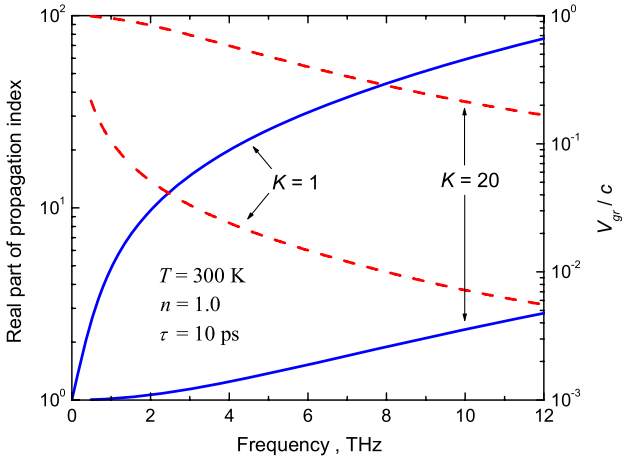

Figure 9. Frequency dependences of the real part of the SP propagation index (solid lines) and the normalized group velocity (dashed lines) for an SGL structure ($K = 1$) and an MGL structure ($K = 20$) at $\varepsilon_F^T = 20$ meV.

values of the quasi-Fermi energy) the absorption coefficient in the SLG structures even with short momentum relaxation times can become negative, although at higher frequencies (see figure 8). Indeed, as seen from figure 8, SPs with the frequencies $\omega/2\pi = 15$–25 THz can be amplified in SGLs with rather short electron and hole momentum relaxation times ($\tau = 0.1$ ps) if $\varepsilon_F^T > 40 - -55$ meV.

4.3. Comparison of SGLs and MGLs

In figures 9 and 10, we compare the real parts of the SP propagation index, absorption coefficients, and the SP group velocities in the optically pumped SGLs and MGLs ($\varepsilon_F^T = 20$ meV). As seen, the SP characteristics in SGLs and MGLs are markedly different. In particular, SGLs exhibit substantially stronger (about 50 times in the peaks) amplification (higher plasmon gain) in a wide frequency range (from 4 to 8 THz) at $\tau = 10$ ps. This is attributed to markedly different values of the SP group velocities in SGLs (relatively small plasmon group velocity) and in MGLs (in which this velocity is relatively high), as shown in figure 9, which, in turn, is due to different net electron and hole densities and different widths of the SP electric field localization that are clearly seen in figure 11. An example of the dependence of the SP

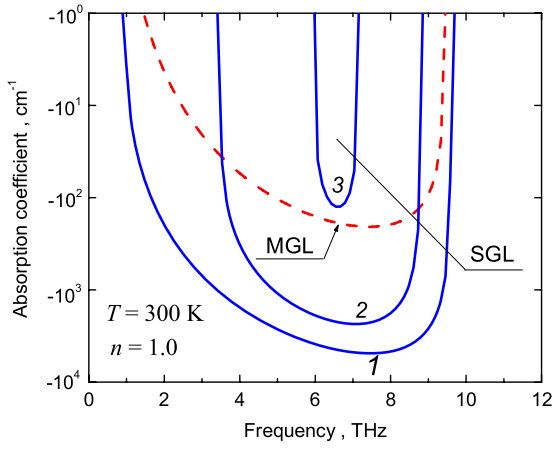

Figure 10. Frequency dependences of the SP absorption coefficient at $\varepsilon_F^T = 20$ meV for an SGL structure with 1—$\tau = 10$ ps, 2—$\tau = 1.0$ ps, and 3—$\tau = 0.54$ ps, and for an MGL structure with $K = 20$ (dashed line) and $\tau = 10$ ps.

absorption coefficient in the structures with optically pumped GLs on the number of layers is demonstrated in figure 12. Thus, at the same values of the optical pumping intensity

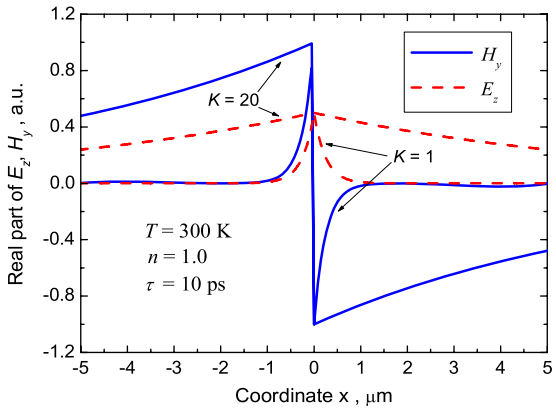

Figure 11. Spatial distribution of the real parts of the SP electric and magnetic fields in an SGL structure and MGL structures with $K = 20$ at $T = 300$ K, $\varepsilon_F^T = 20$ meV, $\tau = 10$ ps and $\omega/2\pi = 6$ THz.

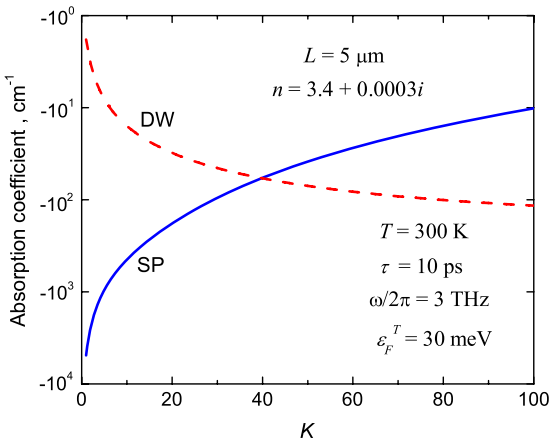

Figure 12. Absorption coefficients of SPs (solid line) and an electromagnetic mode (dashed line) in a dielectric waveguide (DW) [6] as functions of the number of GLs, K.

and the electron and hole momentum relaxation time, SPs in SGL structures can exhibit stronger amplification than MGL structures. However, as demonstrated [15, 27], the momentum relaxation time in epitaxially grown MGLs can be rather long, so MGL structures might be preferable in applications. Taking into account the real possibility of a large difference in the electron and hole relaxation times in SGL and MGL structures, in figure 10, we demonstrate that the SP amplification in the MGL structure with $K = 20$ and $\tau = 10$ ps can exceed that in the SGL structure with smaller τ. Hence, to achieve the SP maximum gain, the number of GLs should be optimal.

A decrease in the SP gain with increasing K is in contrast to the behavior of the electromagnetic modes in the optically pumped MGL structures with dielectric waveguides considered by us previously [6]. For comparison, the pertinent dependence taken from [6] for the waveguide thickness $L = 5$ μm (at the same quality of GLs and pumping conditions) is shown in figure 12 as well.

5. Conclusions

We studied the SPs in optically pumped SGL and MGL structures. Using the developed model, we calculated the SP dispersion relations, spatial distributions of their electric and magnetic fields, and frequency dependences of the absorption coefficient as functions of the optical pumping and factors determining the intraband absorption in the GLs and the substrate. It was demonstrated that at sufficiently strong but realistic optical pumping, the SP absorption coefficient can be negative (so that the gain is positive) in a certain range of frequencies. The absolute value of the SP absorption coefficient (plasmon gain) in an SGL structure can be fairly large and markedly exceed the gain of electromagnetic modes in dielectric waveguides with optically pumped SGL or MGL structures. In contrast to the cases of amplification of electromagnetic modes in the structures with optically pumped SGLs and MGLs and dielectric waveguides, the SP amplification weakens with increasing number of GLs, K. However, due to the possibility of rather long momentum relaxation times of electrons and holes in MGL structures, the SP maximum gain can be achieved at optimal values of the number of GLs. The effect of SP amplification in optically pumped SGL and MGL structures can be used in THz lasers (with the conversion of SPs to output electromagnetic modes). The variation of the SP characteristics by optical pumping might be useful in different GL-based plasma-wave devices.

Acknowledgments

The authors are grateful to M Ryzhii for comments. This work was supported by the Japan Science and Technology Agency, CREST, Japan and partially by the Federal Russian Program ‘Scientific and Educational Staff’, Russia.

References

[1] Ryzhii V, Ryzhii M and Otsuji T 2009 *J. Appl. Phys.* **101** 083114
[2] Satou A, Vasko F T and Ryzhii V 2008 *Phys. Rev.* B **78** 115431
[3] Castro Neto A H, Guinea F, Peres N M R, Novoselov K S and Geim A K 2009 *Rev. Mod. Phys.* **81** 109
[4] Dubinov A A, Aleshkin V Ya, Ryzhii M, Otsuji T and Ryzhii V 2009 *Appl. Phys. Express* **2** 034509
[5] Ryzhii V, Ryzhii M, Satou A, Otsuji T, Dubinov A A and Aleshkin V Ya 2009 *J. Appl. Phys.* **106** 084507
[6] Ryzhii V, Dubinov A A, Otsuji T, Mitin V and Shur M S 2010 *J. Appl. Phys.* **107** 054505
[7] Rana F 2008 *IEEE Trans. Nanotechnol.* **7** 91
[8] Ryzhii V 2006 *Japan. J. Appl. Phys.* 2 **45** L923
[9] Vafek O 2006 *Phys. Rev. Lett.* **97** 266406
[10] Falkovsky L A and Varlamov A A 2007 *Eur. Phys. J.* B **56** 281
[11] Ryzhii V, Satou A and Otsuji T 2007 *J. Appl. Phys.* **101** 024509
[12] Hwang E H and Das Sarma S 2007 *Phys. Rev.* B **75** 205418
[13] Hanson G W 2008 *J. Appl. Phys.* **103** 064302
[14] Jablan M, Buljan H and Solijacic M 2009 *Phys. Rev.* B **80** 245435
[15] Orlita M and Potemski M 2010 *Semicond. Sci. Technol.* **25** 063001
[16] Vasko F T and Ryzhii V 2008 *Phys. Rev.* B **77** 195433
[17] Xia F, Mueller T, Lin Y-m, Valdes-Garcia A and Avouris F 2009 *Nature Nanotechnol.* **4** 839

[18] Ryzhii V, Ryzhii M, Mitin V and Otsuji T 2010 *J. Appl. Phys.* **107** 054512
[19] Ryzhii V, Ryzhii M, Mitin V and Shur M S 2009 *Appl. Phys. Express* **2** 034503
[20] Ryzhii M, Ryzhii V, Otsuji T, Mitin V and Shur M S 2010 *Phys. Rev.* B **82** 075419
[21] Varchon F *et al* 2007 *Phys. Rev. Lett.* **99** 126805
[22] Ryzhii V, Ryzhii M and Otsuji T 2008 *Phys. Status Solidi* c **5** 261
[23] Ryzhii V, Ryzhii M, Mitin V, Satou A and Otsuji T 2011 arXiv:1102.2026 [cond-mat.mes-hall]
[24] Satou A, Otsuji T and Ryzhii V 2010 Abstract *ISGD2010: 2nd Int. Symp. on Graphene Devices: Technology, Physics, and Modeling (Sendai, Oct. 2010)*
[25] Falkovsky L A and Pershoguba S S 2008 *Phys. Rev.* B **103** 064302
[26] Peres N M R 2010 *Rev. Mod. Phys.* **82** 2673
[27] Neugebauer P, Orlita M, Faugeras C, Barra A-L and Potemski M 2009 *Phys. Rev. Lett.* **103** 136403
[28] Oliner A A and Tamir T 1962 *J. Appl. Phys.* **33** 231
[29] Novotny L and Hafner C 1994 *Phys. Rev.* E **50** 4094
[30] Palik E D 1998 *Handbook of Optical Constants of Solids* (New York: Academic)